THE UNIVERSITY *of* EDINBURGH

Edinburgh Research Explorer

Molecular Simulations of Kinetic-Friction Modification in Nanoscale Fluid Layers

OPEN ACCESS

Molecular Simulations of Kinetic-Friction Modification in Nanoscale Fluid Layers**

M.R. Farrow,[1] A. Chremos,[2] P.J. Camp,[1] S.G. Harris[3] and R.F. Watts[4]

[1]EaStCHEM, School of Chemistry, Joseph Black Building, University of Edinburgh, West Mains Road, Edinburgh, EH9 3JJ, UK.

[2] Department of Chemical Engineering, Princeton University, Princeton, NJ 08540, USA.

[3]Infineum UK Ltd, Milton Hill Business and Technology Centre, P.O. Box 1, Abingdon, Oxfordshire, OX13 6BB, UK.

[4]Infineum USA LP, 1900 E Linden Avenue, Linden, NJ 07036, USA

[*]Corresponding author; e-mail: philip.camp@ed.ac.uk

Abstract

Molecular simulations are used to explore kinetic-friction modification in nanoscale fluid layers of oil and additive confined between sheared parallel walls. The molecules are represented by coarse-grained bead-spring models that reflect the essential solvophilic and solvophobic natures of the chemical groups. The degree of friction modification is surveyed as a function of wall separation, sliding velocity, additive molecular weight and architecture, and oil–additive composition. As a rule, the kinetic-friction coefficient is found to increase first linearly and then logarithmically with increasing sliding velocity. From the results for different additive molecules, some subtle but systematic effects are found that point towards an optimum molecular weight and architecture.

1. Introduction

The control of friction in complex fluids is of paramount importance to the automotive industry, amongst others. The reduction of friction between sliding metal contacts is obviously a key target for the control and minimisation of wear [1, 2]. In other circumstances, however, it is desirable to increase the kinetic friction between surfaces lubricated with fluids (typically oils) [3]. The development of kinetic friction between parallel moving surfaces is dictated by the generation of a lateral force resisting the motion, and the transmission of a normal force (load) across the lubricating fluid layer. Adding small amounts of an appropriate additive to the base oil can modify the forces mediated by the thin fluid layer confined between parallel surfaces but without compromising the properties of the bulk fluid. It is fair to say that, at present, the development of such additives is largely heuristic and relies on exploiting existing chemistries to generate putative molecules for testing. In principle it should be possible to study friction using molecular-scale simulations and eventually to use these techniques to yield predictions for additives with optimal friction properties. Seminal work in molecular simulations of flow and friction in polymer melts/solutions in slit pores has been performed by Robbins and co-workers [4, 5, 6, 7, 8, 9, 10]. Amontons' Laws (friction force is proportional to applied load and independent of the apparent contact area), Coulomb's law (kinetic friction force is independent of sliding velocity), and the molecular-scale origins of static and kinetic friction have been thoroughly discussed in the context of simple molecular models of idealised surfaces and lubricating fluids, with and without surface adsorption of fluid molecules [5, 6, 7, 11].

In the presence of a lubricating fluid layer, the nature and strength of the interactions between fluid molecules and the surfaces clearly affect frictional properties. When the surface separation approaches molecular dimensions, the fluid layer provides boundary lubrication and the resulting kinetic frictional force is roughly independent of sliding velocity [11]. The spatial organisation of the molecules in such thin layers can be very high [11] but it can be frustrated by oscillatory shear motions with periods

comparable to molecular relaxation times [12]. If molecules are pinned (chemisorbed) to one or both of the surfaces, then again a high degree of molecular organisation takes place as the surfaces are sheared [13]. For strongly physisorbed molecules the application of shear causes molecules to flatten near the surface and ultimately leads to desorption [14, 15]. So-called 'stick-slip' sliding can occur when long polymer chains are strongly confined and adsorption contacts are possible simultaneously on both surfaces [16]. Stick-slip sliding also occurs in thicker polymer films at high sliding velocities and it leads to the kinetic frictional force increasing apparently logarithmically with velocity [6]; such complicated behaviour can be described using 'rate-state' equations [17, 18, 19, 20, 21].

Whilst fully atomistic simulations of lubrication and friction over the relevant lengthscales and timescales are still relatively rare due to current computing capabilities [22, 23, 24, 25, 25], so-called coarse-graining strategies routinely allow the simulation of chemically resolved molecular models with a sufficient reduction in computational overhead to make realistic situations accessible. Roughly speaking, coarse-graining involves replacing groups of bonded atoms in a molecule with one representative blob or bead; the interactions between different beads are then prescribed so as to mimic the net interactions in a real material of interest.

This work is focused on coarse-grained simulations of kinetic-friction modification in oily fluids confined between parallel plates (slit-pore geometry). Emphasis is placed on the friction modification in the hydrodynamic regime at high sliding velocities (in contrast to the boundary-friction regime at low sliding velocities). A great deal is known about the molecular mechanisms of boundary-friction reduction by additives, but a secondary effect is how additives modify the kinetic friction in the hydrodynamic regime. The aim of this study, therefore, is to determine structure-property relationships concerning friction modification by additives at high sliding velocities. The coarse-grained models to be studied are inspired by common lubricant additives developed and marketed by Infineum UK Ltd [26]. The chemical details of these additives are confidential, but in broad terms the additives are chain-like molecules of morphology ABA, where A represents an aliphatic chain (typically consisting of 10-50 carbon atoms) and B represents a polar section. The essential point is that, when dispersed in a hydrocarbon oil, the polar sections will experience a net solvophobic attraction which is directly analogous to the hydrophobic attraction experienced by non-polar solutes in aqueous solution [27]. In addition, the polar section may be comprised of surface-active chemical groups which lead to a net attraction with metal, metal-oxide, or polymeric surfaces. The overall aim of this study is to calculate kinetic friction coefficients from coarse-grained molecular-dynamics simulations of a fluid layer trapped between moving parallel surfaces, and to gain insight on the molecular-scale structure and organisation of the oil and additives within the lubricating layer.

This article is organised as follows. The molecular models and simulation methodology are summarised in section 2. The results are presented in section 3 and are organised in order to show the

effects of additive molecular weight and architecture (section 3.3) and composition (section 3.4). A summary is presented in section 4.

2. Model and simulation methods

A coarse-grained, bead-spring model was employed to represent the constituent molecules. In general terms, coarse-graining is achieved by replacing each region of a complex molecule by a soft bead, and subsequently linking different beads together with a suitable spring [28, 29, 30]. For example, in the coarse-grained model of a long-chain alkane, each bead might represent several $-CH_2-$ and/or $-CH_3$ groups. The physical justification is that, on average, a subset of bonded atoms occupies a roughly spherical volume. Over the last two decades, this type of approach has been employed in a diverse range of applications, including polymers, block copolymers, surfactants, polypeptides, and polyelectrolytes; the scope of coarse-graining methods is vast [31, 32] but there has yet to be established a robust protocol for developing specific coarse-grained models. One of the reasons for this is that the effective interactions between beads are mediated by large numbers of atoms, and hence the effective interaction potential depends on thermodynamic properties like temperature and density. Nonetheless, unique insights on the properties of complex fluids can be obtained by using physically and chemically inspired models of the constituent molecules. Although the properties of such model systems cannot always be related directly to those of real materials, qualitative and semi-quantitative information can be obtained which is of immediate practical relevance.

To guide the following description, a schematic diagram and typical snapshot of the system are shown Figure 1. The system was built up from two types of bead: solvent molecules were made from 'A' beads; additive molecules were made up of A beads (representing solvophilic groups) and B beads (representing solvophobic groups); and the (generally polar) surfaces were made from B beads. Two parallel, planar walls with dimensions $L_x \times L_y$ were separated by a distance L_z: the direction normal to the walls was designated the laboratory z axis and so the walls were at $z = \pm L_z/2$. Each wall was constructed from a rigid hexagonal close packed layer of B beads with a lattice spacing of $2^{1/6}\sigma$, where σ is the bead diameter (to be defined below).
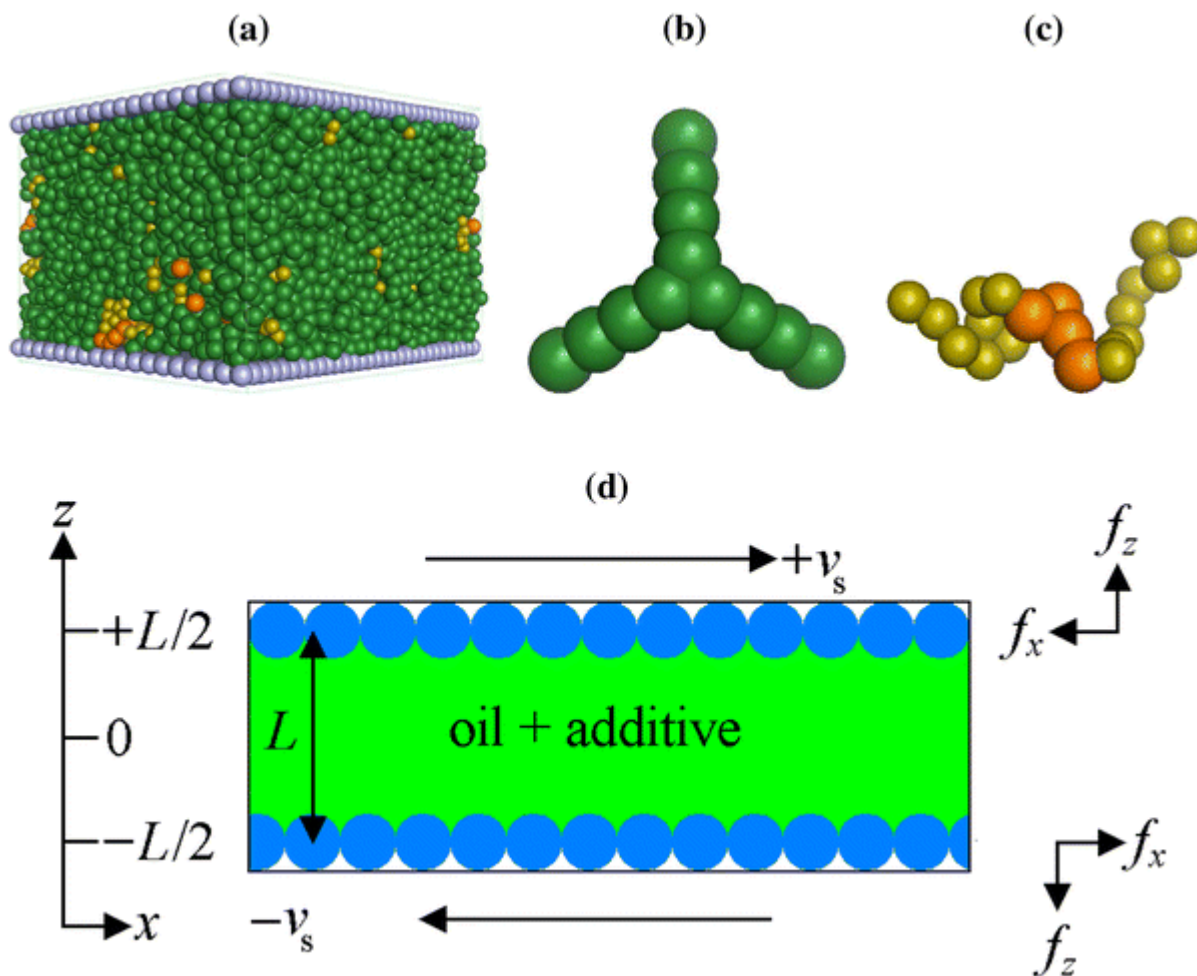
Figure 1. a Snapshot of a simulation configuration with $L\,z = 20\,\sigma$. The oil A beads are shown in green, the additive A beads in yellow, the additive B beads in orange, and the wall B beads in blue. **b** An oil molecule composed of 13 A beads. **c** An $A_8B_4A_8$ additive molecule. **d** Schematic diagram of the system geometry, the shearing motion of the walls, and the forces acting on the beads of the walls

The fluid molecules are complex. Branched-alkane oil molecules were represented as three-armed star polymers made up of A beads; see Figure 1b. The additive molecules were represented as block copolymers, each polymer consisting of solvophilic (A) beads and solvophobic (B) beads connected in the fashion $A_nB_4A_n$ or $A_{2n}B_4$ where $n = 4, 8, 20$; see Figure 1c. The numbers of beads to be used in rendering the molecules were determined by comparing the bead structures to space-filling models generated using molecular mechanics energy minimization, with the aim of capturing the length-to-breadth ratios of the chain-like segments within the molecules. The molecular mechanics calculations were performed for individual additive molecules [26] in vacuum using the COMPASS force field in Accelrys Materials Studio 4.2 [33]. In practice, matching beads with the energy-minimized molecular structures led to an effective bead diameter σ in the region of 3.5 Å; given that a carbon-carbon bond

length is around 1.5 Å, one coarse-grained bead represents a portion of a chain containing, on average, 2.5 carbons.

2.1. Interactions

A liquid is a very dense state of matter, and the short-range repulsive interactions between molecules largely dictate the microscopic, spatial and temporal correlations between molecules [34]. In other words, liquids are so dense that packing effects largely account for their properties. Therefore, to represent the structure and dynamics of a molecular fluid, it is sufficient to include only the short-range repulsive forces. Of course, in real liquids the attractive potential energy is considerable, but because molecules can never get beyond interaction range of their neighbours, this attraction merely provides a kind of 'uniform background'. In an oily, non-polar solvent, polar solutes cluster as if there are additional attractive forces in excess of those experienced by isolated molecules. This is due to the fact that the non-polar solvent poorly solvates polar groups, and hence the polar groups will tend to aggregate. In a similar manner, polar groups will experience attractive forces due to the polar wall groups. These tendencies to aggregate are represented with the addition of attractive terms to the effective interaction potentials. This situation is analogous to the hydrophobic attraction which gives rise to clustering of non-polar solutes in water (a strongly polar solvent) [27].

As mentioned in section 2, in the present case the beads are divided in to two classes: A beads that make up the oil and the aliphatic chains of the additives; and B beads that make up the additives' polar sections and the walls. The effective bead-bead interactions can be described in terms of the Lennard–Jones potential

$$V_{LJ}(r) = 4\epsilon \left[\left(\frac{\sigma}{r} \right)^{12} - \left(\frac{\sigma}{r} \right)^6 \right] \tag{1}$$

where ϵ is the potential-energy well depth and σ is the range parameter which can be loosely interpreted as the bead diameter. The effective BB interactions are attractive compared to the effective AB and AA interactions and so the full LJ potential is used. The attractive tail is insignificant beyond a diameter of $2 - 3$ σ and so to reduce the number of interactions which have to be computed in the simulations, the potential was truncated at $r_c = 2.5$ σ; to remove the resulting discontinuity the potential is shifted so that it is equal to zero at the cut-off distance. The cut-and-shifted potential employed is therefore

$$V_{BB}(r) = \begin{cases} V_{LJ}(r) - V_{LJ}(r_c) & r \leq r_c \\ 0 & r > r_c \end{cases} \qquad (2)$$

In the coarse-graining scheme, the effective AA and AB interactions are ambivalent in the sense that they are not as favourable as the BB interactions. Hence, the effective AA and AB interactions were set to be purely repulsive. This was achieved by truncating and shifting the LJ potential at the position of the minimum, i.e., $r_0 = 2^{1/6} \sigma$:

$$V_{AA}(r) = V_{AB}(r) = \begin{cases} V_{LJ}(r) + \epsilon & r \leq r_0 \\ 0 & r > r_0 \end{cases} \qquad (3)$$

This is the Weeks–Chandler–Andersen potential [35]. A spring-like potential was needed for describing the bonded beads. This can be modelled by a non-linear spring potential which limits the bond length under very large forces (mimicking the constraints of chemical bonds). The most widely used 'bonding' interaction in polymer simulations is the finitely extensible non-linear elastic (FENE) potential which reads

$$V_{intra}(r) = \begin{cases} -\frac{1}{2}\kappa R_0^2 \ln\left(1 - \frac{r^2}{R_0^2}\right) & r < R_0 \\ \infty & r \geq R_0. \end{cases} \qquad (4)$$

The values for the parameters were $R_0 = 1.5\ \sigma$ and $\kappa = 30\epsilon/\sigma 2$, which have proven useful in practice [28, 29, 30] and are almost universally adopted in coarse-grained simulations of polymer-like molecules. Note that the particular choice of interaction parameters for the fluid molecules will not have a strong effect on the measured friction. This was first shown by He and Robbins in their studies of static and kinetic friction in thin films [6]. The fluid-wall interactions have been shown to have a greater effect on slip and friction [4,25, 36]. We conducted some of our own tests, such as doubling the strength of surface-additive attractions, but no strong dependence of the measured kinetic-friction coefficients on parameters was observed. Therefore, the interaction parameters employed here provide a representative set of results with which to explore the dependence of kinetic friction on such properties as wall separation, sliding velocity, additive molecular weight and architecture, and oil–additive composition.

2.2. Langevin Dynamics

The model system was simulated using Langevin dynamics in which the particles in the fluid experience random and drag forces as well as the conservative interaction forces derived from the interaction potentials. These forces serve to thermalise the system and hence regulate the temperature. This is a technical necessity because when shear is applied, work is done on the system and energy is dissipated as heat. Without a thermostat, the system temperature would increase without limit. Therefore the random and drag forces in this situation are fictional, and merely serve to maintain a constant temperature. The effects on the bead dynamics are minimal, however, because the associated friction constant is kept as low as possible whilst maintaining reasonable temperature control. The equations of motion for the fluid beads are

$$m\ddot{r}_i = -\nabla V_i - m\Gamma(0, \dot{y}_i, \dot{z}_i) + (0, W_y, W_z) \qquad (5)$$

where m is the bead mass (assumed to be the same for all beads), $2r_i$ is the position of bead i, Γ is the Langevin friction coefficient, W_y and W_z describe random, Brownian forces of the heat bath acting on each bead, and V_i is the potential energy of particle i from which the force $(-\nabla V_i)$ is derived. To effect shear, the walls were moved in the x-direction with constant velocities $\pm v_s$ and infinite inertia (zero acceleration). See Figure 1d for a schematic diagram of the system geometry. The frictional and Brownian forces given by the second and third terms of Eq. 5, respectively, were only applied in the y and z directions in order that there are no adverse affects on the velocity field in the direction of shear (x) [4, 6]. The potential energy is given by a sum over pairwise additive interactions, i.e., $V_i = \sum_{j \neq i}^{N} V_{ij}$, V_{ij} being the interaction energy between beads i and j. $W_y(t)$ and $W_z(t)$ are represented by Gaussian white noise satisfying the fluctuation–dissipation theorem [37]:

$$\langle W_\alpha(t) W_\beta(t') \rangle = 2k_B Tm\Gamma \delta_{\alpha\beta}\delta(t - t') \qquad (6)$$

Implementation details of the Langevin-dynamics method and bead-spring models are explained in Refs. [28–30].

The simulations were conducted in reduced units defined as follows: temperature $T* = k_B T/\epsilon$; reduced density $\rho^* = N\sigma^3/V$ where N is the total number of beads in the simulation volume V; reduced time $t^* = t/\tau$ where $\tau = \sqrt{m\sigma 2/\epsilon}$. In all cases, the simulation cell was cuboidal with periodic boundary conditions applied in the plane parallel to the walls; no periodic boundary conditions were applied normal to the walls in order that molecules could not interact 'through the wall' with periodic images. The equations of motion were integrated using the velocity-Verlet algorithm and with a time step in

the range $0.005 \leq \delta t^* \leq 0.01$, depending upon the sliding velocity. The reduced temperature $T* = kBT/\epsilon$ was 1.0; the temperature dependence of frictional properties has been shown to be weak [6]. The bead friction coefficient was set at $\Gamma = 0.5/\tau$ (a small value), but as mentioned above, in our case it is used merely as a thermostat. The choices of these parameters ensure that the bonds between monomers do not pass through each other during one integration time step and that the temperature is well controlled for sliding velocities up to $v_s = 0.1 L_z/\tau$. Equilibration runs consisted of $\sim 10^5$ timesteps, whilst production runs (over which observables were measured and averaged) consisted of 2×10^5 timesteps.

2.3. Model System Parameters

We have studied oil with and without additive molecules; the additive molecules are either low molecular weight ($A_4B_4A_4, A_8B_4$), medium molecular weight ($A_8B_4A_8, A_{16}B_4$), or high molecular weight ($A_{20}B_4A_{20}$). For the oil–additive mixtures, the composition was adjusted so that 90% of the beads were oil and the remaining 10% of the beads were additive; experimentally, this corresponds to a 10% v/v solution of additive in oil, which is typical in applications. (For brevity we refer to this composition as 10% v/v.) To assess concentration effects, we have also studied some systems with compositions corresponding to equal volume fractions of B beads. For each fluid, we have studied three different wall separations, $L_z/\sigma = 10$, 20, and 40; the other box dimensions were $L_x = 50\ \sigma$ (in the sliding direction) and $L_y = 20\ \sigma$. For each fluid and wall separation, we have simulated a range of sliding velocities v_s.

A typical mass density for a C_{30} oil is 0.8 g cm^{-3} and assuming a molecular weight of around 420 g mol^{-1} this corresponds to a number density of approximately 1.15×10^{27} molecules m^{-3}. In the coarse-graining scheme employed here, 30 CH_2/CH_3 groups equate to 12 beads; the oil molecule is therefore constructed from three chains of four beads, attached to a central bead. Each oil molecule consists of 13 beads, and so the number density of beads is $\rho \simeq 1.49 \times 10^{28}$ m^{-3}. In reduced units (with $\sigma \simeq 3.5$ Å) this number density is $\rho^* = \rho\sigma^3 \simeq 0.65$; we adopted this value throughout. The number of fluid beads in the system ranged between 6.5×10^3 (with $L_z = 10\ \sigma$) and 2.6×10^4 (with $L_z = 40\ \sigma$). Initial fluid configurations were prepared by generating a low-density random configuration of molecules with a large value of L_z, and then slowly compressing the system to the target value of L_z. A reduced temperature $T^* = 1$ means that, at room temperature, $\epsilon = kBT \simeq 4 \times 10{-}21$J. The bead mass is one-thirteenth of the molecular mass of oil, which gives $m \simeq 5.36 \times 10^{-26}$ kg. Therefore, the basic unit of time is $\tau = 1.26 \times 10^{-12}$ s and the basic unit of velocity is $\sigma/\tau \simeq 280$ m s^{-1}.

3. Results

3.1. Dependence of kinetic friction on sliding velocity

The kinetic friction coefficient was calculated by measuring the average lateral and normal forces acting on the beads making up the walls. The system geometry is shown in Figure 1(d). The average force acting on a given wall bead (i) is

$$\langle f_i \rangle = (\langle f_{ix} \rangle, 0, \langle f_{iz} \rangle) \tag{7}$$

where $\langle f_{i\alpha} \rangle$ is the average α component of the force. The walls were sheared in the x direction and so $\langle f_{iy} \rangle = 0$. The kinetic friction coefficient μ is given by

$$\mu = -\frac{\sum_i^{N_s} \langle f_{ix} \rangle}{\sum_i^{N_s} \langle f_{iz} \rangle} \tag{8}$$

where N_s is the number of surface beads in a wall; the values for both walls were averaged.

Figure 2a shows the kinetic friction coefficient μ as a function of sliding velocity v_s for fluids confined between walls with $L_z = 10\,\sigma$. For clarity, results are shown only for pure oil, and for oil–additive mixtures with $A_4B_4A_4$, $A_8B_4A_8$, and $A_{20}B_4A_{20}$. For each of the oil–additive mixtures, the volume fraction of additive corresponds to a 10% v/v composition. The first point to note is that the oil friction is very much higher than in the oil–additive mixtures. This is explained by the fact that each branch on an oil molecule is of order 5 σ in length and so at such a small wall separation, it is difficult for oil molecules to move past one another under the shear flow. The presence of additive dramatically reduces the friction. The additive molecules are chain-like and hence can easily move past the branched oil molecules under shear. This reduces the lateral forces on the walls and therefore leads to a reduction in μ. The second point is that the differences between the results for the various oil–additive systems are very small, at least at this wall separation.
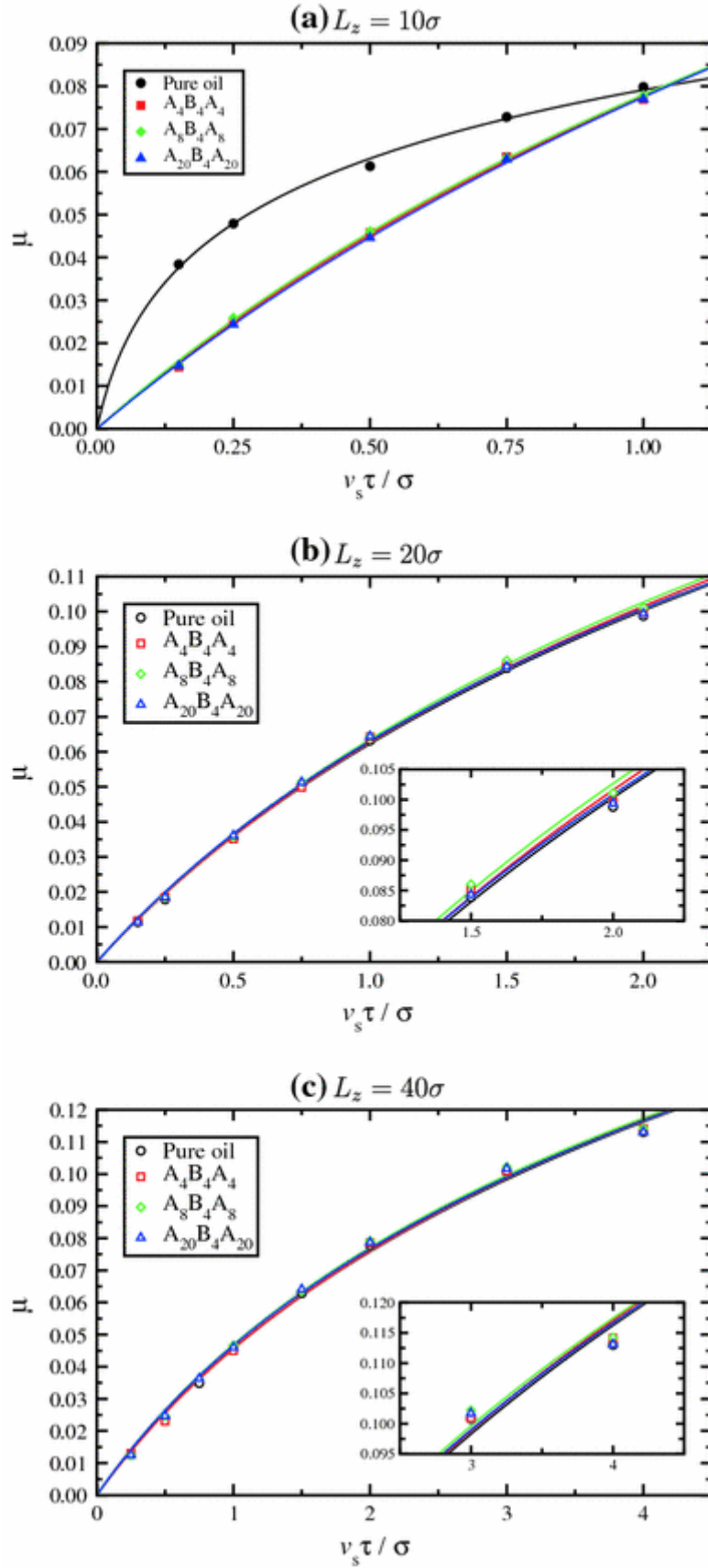
Figure 2. Kinetic friction coefficient μ against sliding velocity v_s for the system with **a** $L_z = 10\,\sigma$, **b** $L_z = 20\,\sigma$, and **c** $L_z = 40\,\sigma$. The points are from simulations and the lines are fits using Eq. 9. Data are

shown for pure oil (*black circles and lines*) and with additive molecules $A_4B_4A_4$ (*red squares and lines*), $A_8B_4A_8$ (*green diamonds and lines*), and $A_{20}B_4A_{20}$ (*blue triangles and lines*)

Figure 2b shows the kinetic friction coefficient for the same four fluids (pure oil and three oil–additive mixtures) confined between walls with $L_z = 20\,\sigma$. Now the pure-oil results are very similar to those for the oil–additive mixtures. The inset to Figure 2b shows that there are now some small but identifiable differences between the pure oil and the oil–additive mixtures. These will be analysed and discussed further below. A similar situation is found at a larger wall separation of $L_z = 40\,\sigma$; the results are shown in Figure 2c. If anything, the differences between the pure oil and the oil–additive mixtures are less pronounced than with $L_z = 20\,\sigma$.

For all systems considered, excellent fits to the data were found to be given by the equation

$$\mu = \mu_0 \ln\left(1 + \frac{v_s}{v_0}\right) \qquad (9)$$

where μ_0 and v_0 are system-specific parameters. A logarithmic dependence of μ on sliding velocity was found in the simulations of He and Robbins [6] and has been observed in experiments [17, 18, 19, 20]. Logarithmic increases in friction with scanning velocity have also been measured in atomistic simulations of friction-force tips on surfaces [38]. A sub-linear dependence of kinetic friction with sliding velocity was also observed in simulations of confined polymers [16] although in that case it was rationalised theoretically as a $v_s^{1/3}$ dependence. The high-v_s logarithmic dependence can be rationalised using an argument inspired by Eyring's description of viscosity in terms of absolute rates [39]. In order to translate parallel to the surface, a fluid molecule (or part of a fluid molecule) near the surface has to overcome energy barriers associated with the microscopic asperities between the surface atoms. When $v_s = 0$ the rates of hopping over a barrier in the $+x$ direction and the $-x$ direction are k_+ and k_-, respectively, and obviously $k_+ = k_-$. The average velocity in the x direction is then

$$\langle v_x \rangle = (k_+ - k_-)d = 0 \qquad (10)$$

where d is a characteristic hopping distance (comparable to the spacing between surface atoms). If the surface is now sliding in the $+x$ direction with velocity v_s, then in an activated-process picture, the rates are altered and the average velocity becomes

$$\langle v_x \rangle = [k_+ \exp\left(\mu f_z d / k_B T\right) - k_- \exp\left(-\mu f_z d / k_B T\right)]d \qquad (11)$$

where fz is, roughly, the normal force exerted on the fluid molecule (or part of the fluid molecule) and $\pm \mu fz d$ is an estimate of the extra work done in overcoming an energy barrier. Clearly, motion is now favoured along the x direction. At very large sliding velocities, $\langle vx \rangle$ is itself very large, and so the first term on the right-hand side of Eq. 11 dominates and we get $\langle vx \rangle \approx [k + \exp(\mu fz d / k_B T)]$. If $\langle vx \rangle \sim vs$ then we obtain

$$\mu \sim \ln v_s \qquad (12)$$

as required. The current simulation data suggest that μ first increases linearly with v_s at low sliding velocities. Equation 9 captures both the low-velocity linear and high-velocity logarithmic behaviours. To demonstrate the quality of the fits, Figure 3 shows a universal plot of μ/μ_0 as a function of v_s/v_0. The collapse of the data on to the universal curve is excellent, although Eq. 9 should perhaps be taken as simply an 'aid to fitting'.
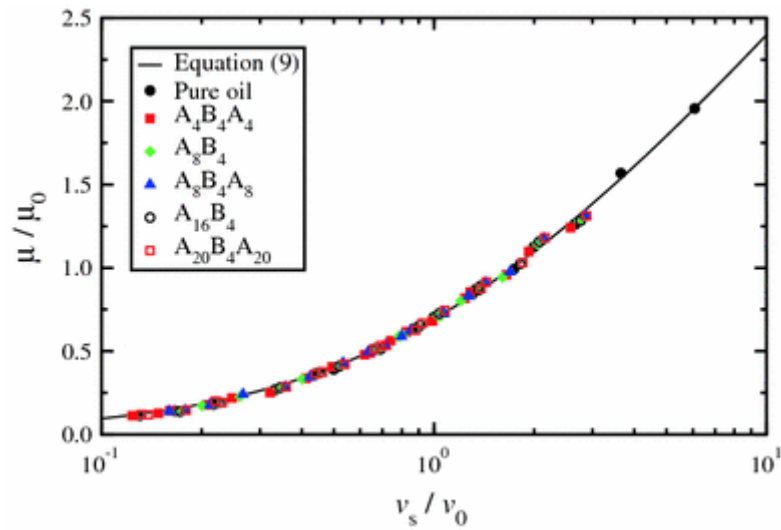
Figure 3. Universal scaling of the kinetic friction shown by plotting μ/μ_0 against v_s/v_0 where μ_0 and v_0 are fitted parameters from Eq. 9

3.2. Slip

The shear rate in the fluid layer depends on the sliding velocity and the degree of slip of the fluid at the walls. The shear rate $\dot{\Gamma}$ is taken to be the gradient of the linear portion of the velocity profile in the centre of the fluid layer ($z = 0$), and is related to v_s and Lz by

$$\dot{\Gamma} = \left.\frac{dv_x}{dz}\right|_{z=0} = \frac{2v_s}{L_z + l_{slip}} \qquad (13)$$

where l_{slip} is the slip length. The connections between slip and the wall structure, fluid-wall interactions, and resulting fluid structure near the walls have been elucidated in molecular simulations of thin polymer films [4, 36]. Recent work on *n*-decane in a 3 nm slit pore formed by face-centred cubic crystals showed that l_{slip} should remain constant ($l_{slip} \simeq 2$ nm) at high sliding velocities ($v_s = 10 -$ 1000 m s^{-1}) [40]. The results from simulations depend sensitively on the how the system is thermostatted. If the simulations are thermostatted correctly, e.g., by applying a Nosé-Hoover thermostat to the wall atoms only, then the plateau in l_{slip} is observed. If, however, only the fluid atoms are thermostatted, then l_{slip} is seen to diverge at high sliding velocities ($v_s \sim 100$ m s^{-1}). Figure 4 shows slip lengths from the current simulations. Firstly, the slip lengths are roughly independent of sliding velocity (except, perhaps, with the two highest values of v_s with $L_z = 40 \sigma$) showing that our Langevin thermostat is largely up to the task. Secondly, the ratio l_{slip}/L_z is O(1), as seen in atomistic *n*-decane simulations [40].

(turn to next page →)
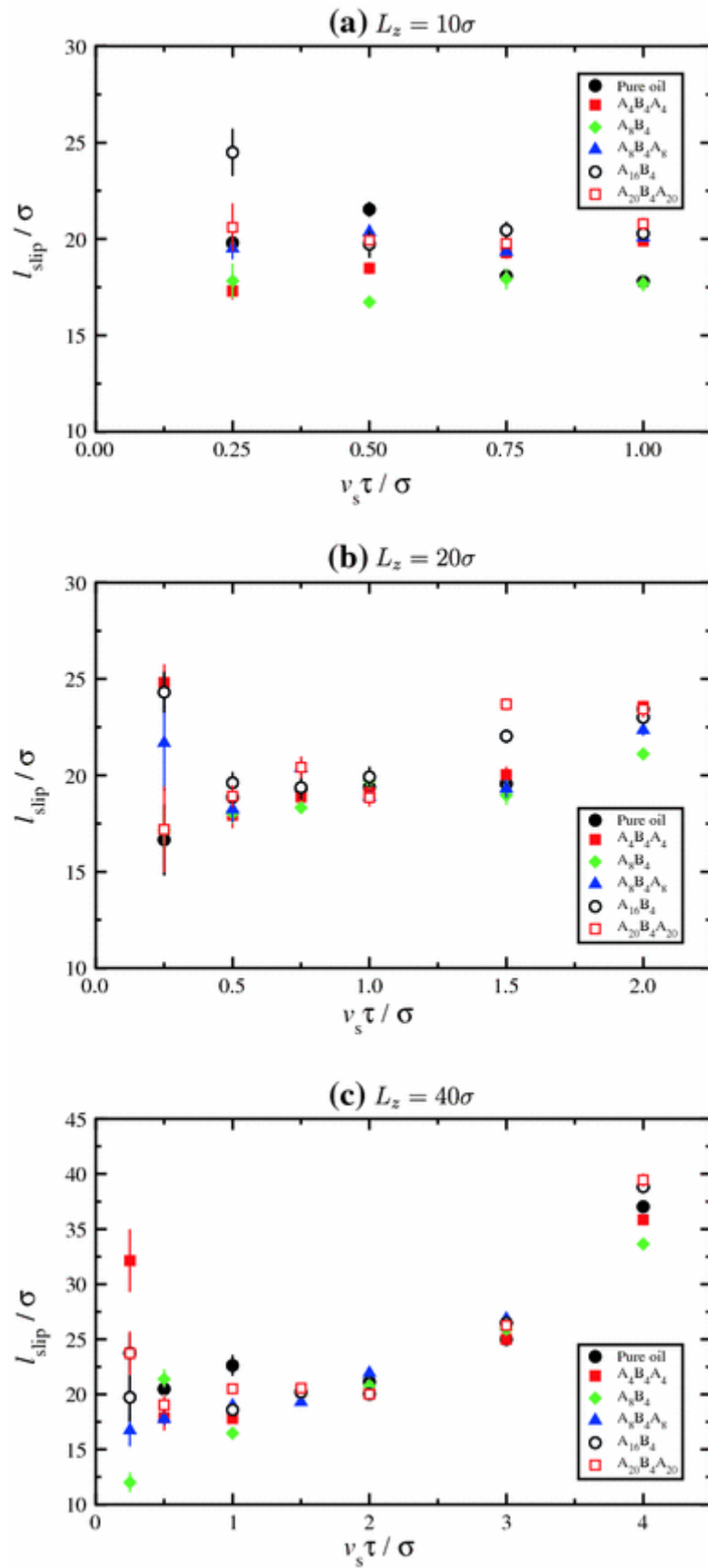
Figure 4. The slip length l_{slip} as a function of sliding velocity v_s for pure oil and oil–additive mixtures: **a** $L_z = 10\ \sigma$; **b** $L_z = 20\ \sigma$; **c** $L_z = 40\ \sigma$

3.3. Effects of molecular weight and architecture on kinetic friction

Attention is now turned to the comparison of kinetic friction in pure oil and in 10% v/v oil–additive mixtures. The effects of molecular weight are assessed by comparing molecules of the same architecture type ($A_nB_4A_n$ or $A_{2n}B_4$) with $n = 4$, $n = 8$ or $n = 20$. The effects of molecular architecture are assessed by a comparison of $A_nB_4A_n$ with $A_{2n}B_4$; the friction coefficients for the $A_{2n}B_4$ molecules were calculated in exactly the same way as reported in the previous section. To carry out these comparisons, the key parameter is clearly the ratio $M = \mu/\mu_{oil}$, where μ and μ_{oil} are the kinetic friction coefficients of an oil–additive mixture and pure oil, respectively.

Figure 5 shows the ratio M against sliding velocity for confined fluids with $L_z = 20\,\sigma$. The simulation results are shown along with the results of the fits from equation 9. The simulation data are subject to large statistical uncertainties at low sliding velocities because here M is the ratio of two small numbers. In general, though, the fits provide a reasonable guide to the eye, at least at high sliding velocities. The variations in M are only on the order of a few percent. Although these are small, they compare favourably with the variations seen in experimental tests carried out by Infineum UK Ltd [26]. The details of these experiments are confidential, but in outline, a range of additives is dissolved in base oil and the lubricant friction is assessed in bench tests at high sliding velocities. The changes in friction upon adding friction modifiers are comparable to those measured here in simulations. As explained in the Introduction, the main aim of these studies is to assess the structure–property relationships of friction modifiers at high sliding velocities, to complement our knowledge of the more familiar boundary-friction behaviour. To this end, some observations can be made regarding the relative performances of the additives.
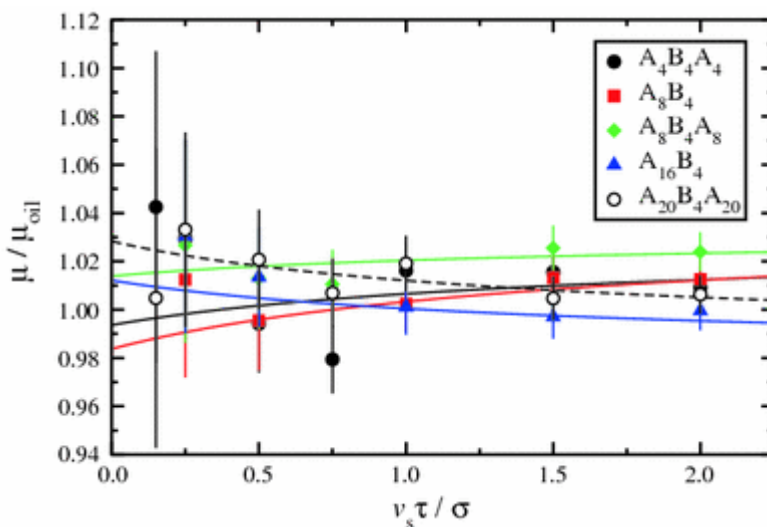
← *Figure 5.* The ratio $M = \mu/\mu_{oil}$ against sliding velocity v_s for the system with $L_z = 20\,\sigma$. The points are from simulations and the lines are derived from the fits to Eq. 9: $A_4B_4A_4$ (*black filled circles and black solid line*); A_8B_4 (*red squares and red line*); $A_8B_4A_8$ (*green diamonds and green line*); $A_{16}B_4$ (*blue triangles and blue line*); $A_{20}B_4A_{20}$ (*black open circles and black dashed line*)

The effects of molecular weight are considered first. The comparison of $A_4B_4A_4$, $A_8B_4A_8$, and $A_{20}B_4A_{20}$ shows that the medium-weight, $A_8B_4A_8$ molecule gives the highest friction. The analogous comparison of A_8B_4 and $A_{16}B_4$ shows that, again, a solvophilic tail of eight A beads leads to the highest friction. A crucial molecular parameter, therefore, appears to be the length of the solvophilic chain(s) (A beads). This is precisely the kind of molecular detail that helps define structure-property relationships for the additives.

One possible explanation may have to do with the degree to which the additives can interact simultaneously with the surface and with the oil. To afford some insight on the distribution of additive throughout the fluid layer, Figure 6 shows some density profiles for the various types of bead at both low and high sliding velocities and with $L_z = 20\,\sigma$. Results are shown for oil A beads, additive A beads, and additive B beads. The local number density of beads of each type $\rho(z)$ is divided by the average density $\langle\rho\rangle$ in order to bring all of the results on to the same scale. Comparing the results for medium-weight $A_8B_4A_8$ and heavy-weight $A_{20}B_4A_{20}$ molecules—Figure 6a–b and c–d, respectively— shows a dramatic qualitative difference in the distribution of additive beads at both low and high sliding velocities. For the medium-weight molecules there appears to be a stratified structure throughout the fluid layer, whilst the heavy-weight molecules show a preference for the surfaces. It appears that the larger molecules elect to form lubricating layers on the surface which ultimately leads to a reduction in kinetic friction between the walls. Figure 7 shows simulation snapshots for these same molecules with $L_z = 20\,\sigma$. Differences between the distribution of additive molecules throughout the fluid layer are not clear from these snapshots, but they do show how an additive 'bridge' may be formed between the two surfaces.
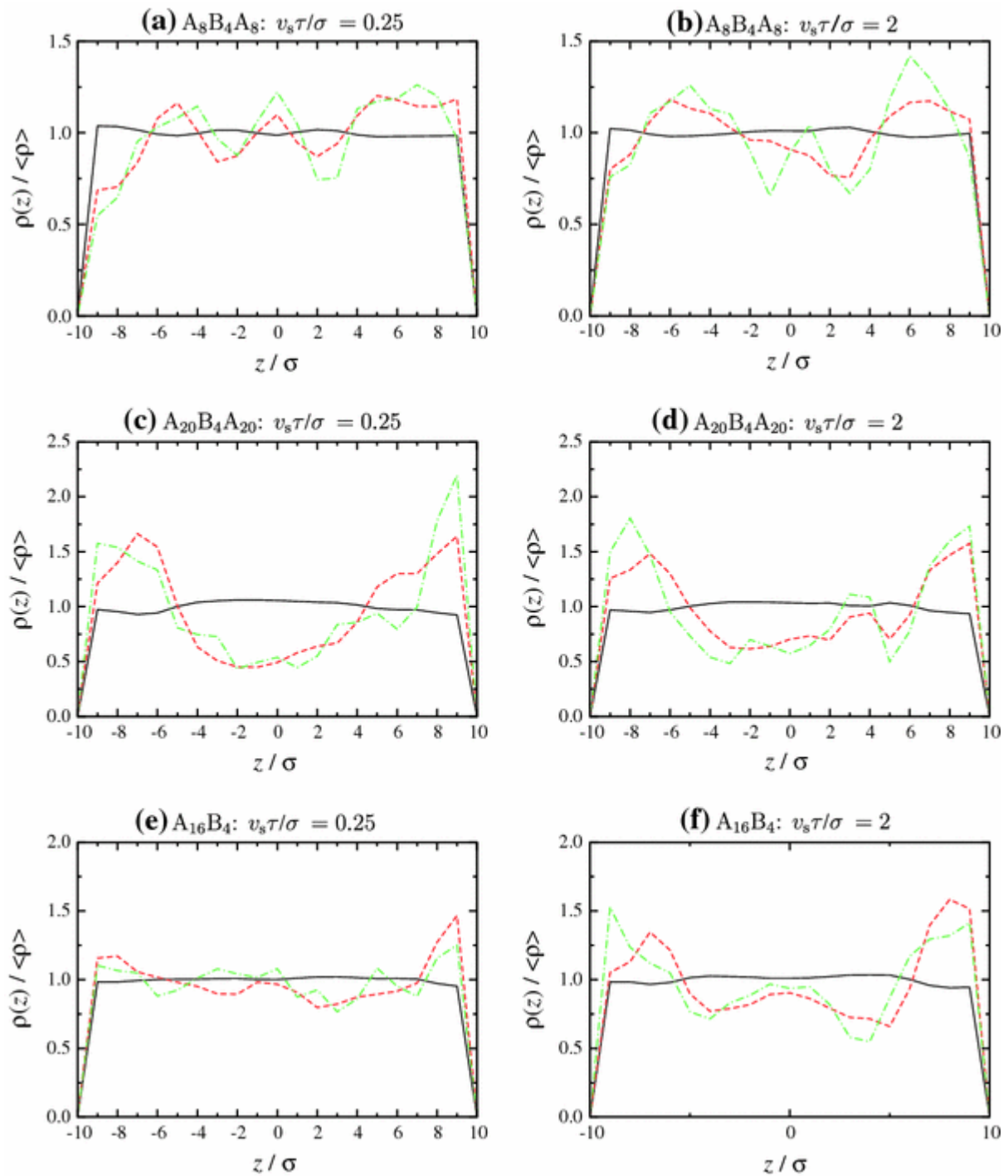
Figure 6. Relative bead density profiles, $\rho(z)/\langle\rho\rangle$, across the layer for systems with $Lz = 20\,\sigma$: **a** $A_8B_4A_8$ and $v_s\tau/\sigma = 0.25$; **b** $A_8B_4A_8$ and $v_s\tau/\sigma = 2$; **c** $A_{20}B_4A_{20}$ and $v_s\tau/\sigma = 0.25$; **d** $A_{20}B_4A_{20}$ and $v_s\tau/\sigma = 2$; **e** $A_{16}B_4$ and $v_s\tau/\sigma = 0.25$; **f** $A_{16}B_4$ and $v_s\tau/\sigma = 2$. The (*black*) *solid lines* are for the oil beads, the (*red*) *dashed lines* are for the additive A beads, and the (*green*) *dot-dashed lines* are for the additive B beads
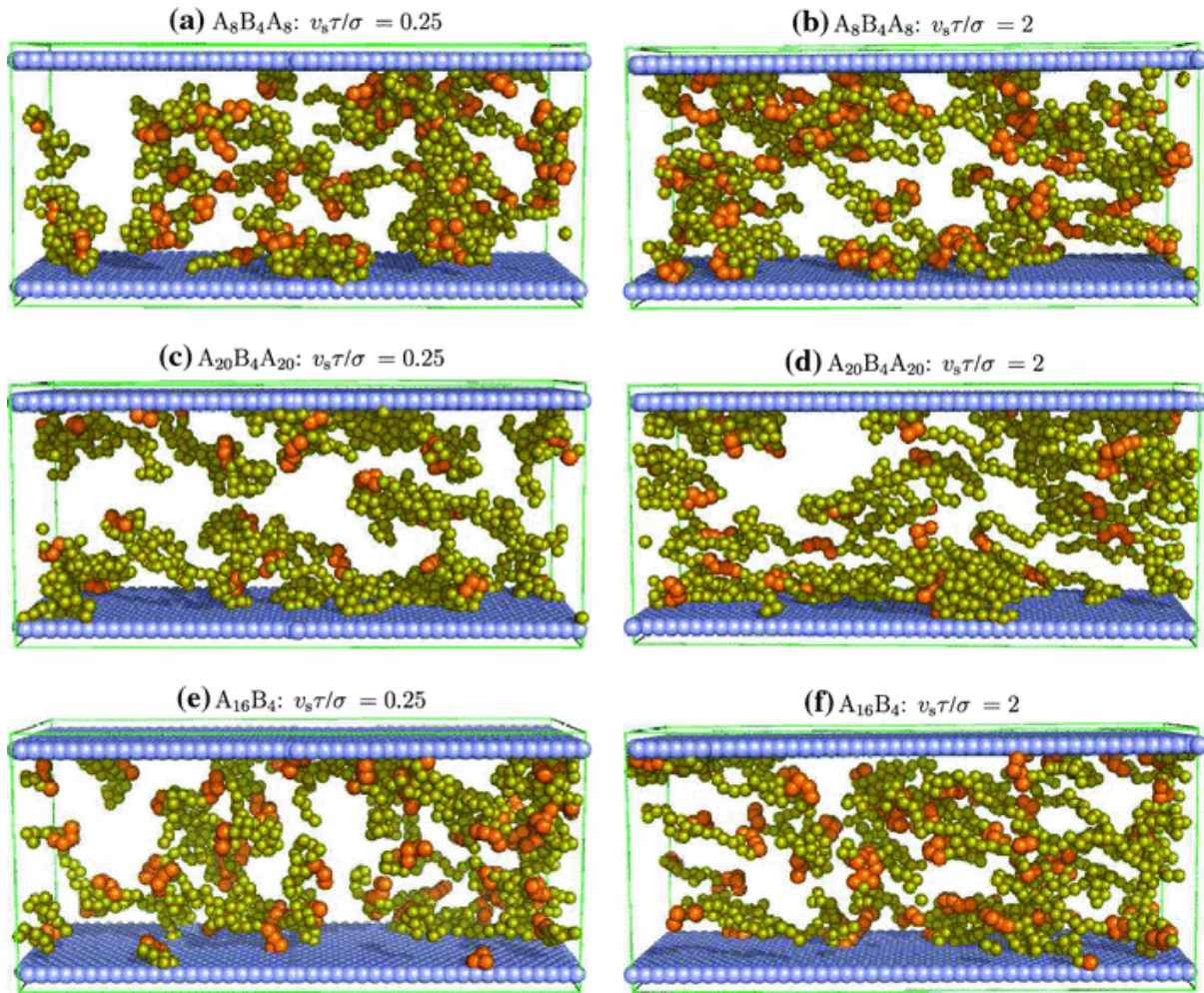
Figure 7. Simulation snapshots of systems with $L_z = 20\ \sigma$: **a** $A_8B_4A_8$ and $v_s\tau/\sigma = 0.25$; **b** $A_8B_4A_8$ and $v_s\tau/\sigma = 2$; **c** $A_{20}B_4A_{20}$ and $v_s\tau/\sigma = 0.25$; **d** $A_{20}B_4A_{20}$ and $v_s\tau/\sigma = 2$; **e** $A_{16}B_4$ and $v_s\tau/\sigma = 0.25$; **f** $A_{16}B_4$ and $v_s\tau/\sigma = 2$. The oil molecules are omitted for clarity

It seems that the organisation of the medium-weight molecules throughout the fluid layer leads to a more effective transmission of force between the walls at high sliding velocities. This optimum situation probably arises from an appropriate balance of the additive–oil interactions (through the solvation of additive A beads) and additive–additive interactions (through the association of B beads). It might also be worth noting that the solvophilic tail of the medium-weight additive is of roughly equal length to two arms of the oil. At high sliding velocities, the oil molecules may extend and the end-to-end length will be approximately 8 bead diameters and this may provide favourable solvation for the solvophilic tails of the $A_8B_4A_8$ molecules. As for the heavy-weight molecules, the question is why they elect to accumulate on the surfaces rather than associate with each other in the bulk. This could be due to the entropic cost of bringing two solvophobic sections together whilst keeping the long solvophilic chains out of the way; in essence, the steric hindrance of the long tails reduces the probability of association for two long molecules. Another contributing factor is that, for a given additive volume fraction, the actual concentration of solvophobic beads is lower for the heavy-weight

molecules than for the medium-weight molecules. Overall, then, it could be more favourable for the B beads in a single heavy-weight molecule to 'associate' with the surface B beads rather than with the B beads on another additive molecule.

The effects of molecular architecture for a given molecular weight can be explored by comparing $A_4B_4A_4$ with A_8B_4, and $A_8B_4A_8$ with $A_{16}B_4$. In the former case, the results for the two molecules in Figure 5 are very similar, at least at high sliding velocity. The comparison in the latter case, however, highlights the special properties of the $A_8B_4A_8$ molecule; it gives a greater increase in friction than the molecule with the same molecular weight but with only one, longer solvophilic tail. Clearly, then, it is better to have two, medium-length solvophilic chains in order to provide a good balance of solubility and interaction between oil and surface. To gain insight on this phenomenon, Figure 6a–b and e–f shows the bead-density profiles for $A_8B_4A_8$ and $A_{16}B_4$, respectively. Some important qualitative differences are evident. As already explained, the $A_8B_4A_8$ molecule organises to form a stratified structure that spans the fluid layer, at both low and high sliding velocities. By contrast, $A_{16}B_4$ molecules are distributed almost uniformly at low sliding velocity, and preferentially at the surfaces at high sliding velocity.

Figure 8 shows the mean-square end-to-end distance $\langle R2 \rangle$ as a function of sliding velocity v_s for the $A_8B_4A_8$ and $A_{16}B_4$ molecules in the $L_z = 20\ \sigma$ system. Clearly, the molecules with shorter solvophilic chains elongate more easily in the shear flow, which should lead to the solvophobic sections being more exposed and available for association. The molecules with longer solvophilic chains elongate less readily, which possibly results in the solvophobic sections being shielded from interactions with each other. To put this in a more quantitative basis, appeal is made to a basic result from polymer physics. The free-energy cost ΔF of extending a freely jointed chain of N links to an end-to-end distance $R \leq N$ is proportional to [41]

$$\Delta F \propto \frac{k_B T R^{5/2}}{N^{3/2}}. \qquad (14)$$
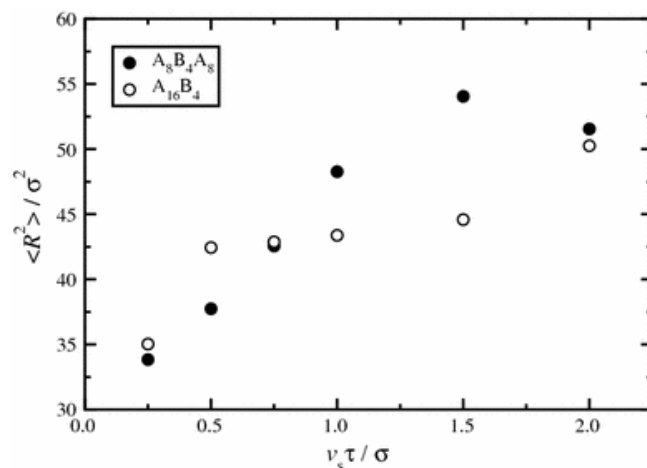
← *Figure 8.* Mean-square end-to-end distance $\langle R2 \rangle$ as a function of sliding velocity v_s for the $A_8B_4A_8$ and $A_{16}B_4$ molecules for the system with $L_z = 20\ \sigma$

The maximal end-to-end distance is clearly proportional to N and so the free-energy cost for full alignment is of order $Nk_B T$. It therefore follows that for a given elongating force, provided by the shear of the fluid layer, short chains will be closer to their full elongation than will long chains. This is because long molecules in globular conformations have very high entropy, and to elongate the molecule and preclude it from accessing the large number of degenerate configurations costs a significant amount of free energy. Now, for additive association to take place, each solvophilic chain individually has to be elongated and for a given force acting on each part of the molecule (arising from the shear flow) it is easier to elongate two short sections than one long one. This may be the underlying cause for the dependence of μ on molecular architecture, but in any case, Figs. 6 and 8 show that the distribution of additive throughout the layer and the elongation of the molecules correlate with an increase in kinetic friction.

Figure 9 shows M as a function of $v_s\tau/\sigma$ for confined fluids with $L_z = 40\ \sigma$. At high sliding velocities, the results are somewhat similar to those with $L_z = 20\ \sigma$, albeit less pronounced. What is clear, though, is that the $A_8B_4A_8$ additive still gives the greater increase in friction. The increase seems to be comparable for a given sliding velocity; if one compares M at $L_z = 20\ \sigma$ and $v_s = 2\ \sigma/\tau$ with M at $L_z = 40\ \sigma$ and the same v_s, then the increase in friction is around 2-3%.
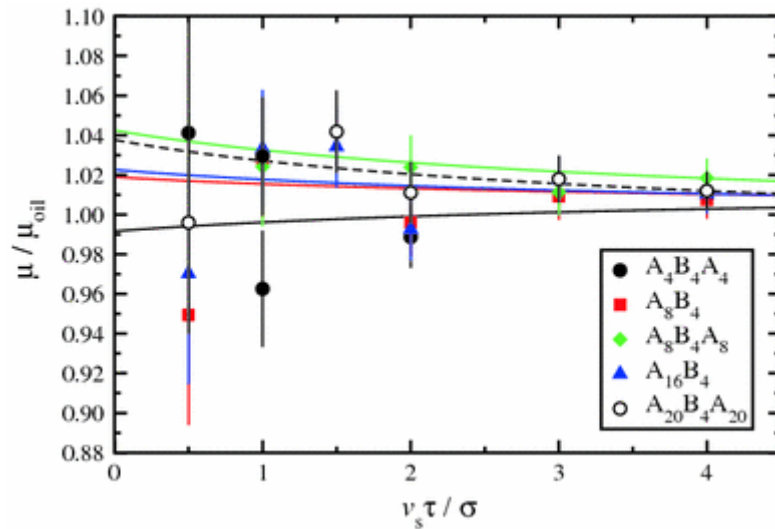
Figure 9. The ratio $M = \mu/\mu_{oil}$ against sliding velocity v_s for the system with $L_z = 40\ \sigma$. The points are from simulations and the lines are derived from the fits to Eq. 9: $A_4B_4A_4$ (*black filled circles and black solid line*); A_8B_4 (*red squares and red line*); $A_8B_4A_8$ (*green diamonds and green line*); $A_{16}B_4$ (*blue triangles and blue line*); $A_{20}B_4A_{20}$ (*black open circles and black dashed line*)

In summary, the results for different additive molecular weights and architectures show that there is a subtle balance between the oil–additive and additive–additive interactions that dictates the organisation of additive throughout the layer and hence modifies the kinetic friction.

3.4. Effects of composition on kinetic friction

The results of the previous section suggest that a crucial factor in the development of kinetic friction modification is the association of solvophobic groups on the additive molecules and the resulting distribution of additive throughout the fluid layer. It is therefore of interest to compare results for different additives at a fixed concentration of solvophobic B beads. To this end we take a 10% v/v solution of $A_8B_4A_8$ in oil as a benchmark and compare it with 6% v/v $A_4B_4A_4$ and 22% v/v $A_{20}B_4A_{20}$ solutions in oil; in each case the volume fraction of B beads corresponds to 2%. Figure 10 shows the kinetic friction coefficient μ as a function of sliding velocity v_s for systems with $L_z = 20\,\sigma$ and $L_z = 40\,\sigma$. Fits from Eq. 9are also included to guide the eye. For both wall separations it is clear that the medium-weight $A_8B_4A_8$molecule provides the most consistent increase in kinetic friction, although its performance is comparable to that of $A_{20}B_4A_{20}$ with the smaller wall separation. Certainly, though, the light-weight $A_4B_4A_4$ molecule is significantly worse than the others. This comparison highlights again the importance of getting the right balance between oil–additive and additive–additive interactions; to achieve the optimum distribution of additive throughout the fluid layer it is not sufficient simply to adjust the additive concentration. There has to be the right balance of additive solvation and additive association, which can be achieved by altering molecular architecture and molecular weight.
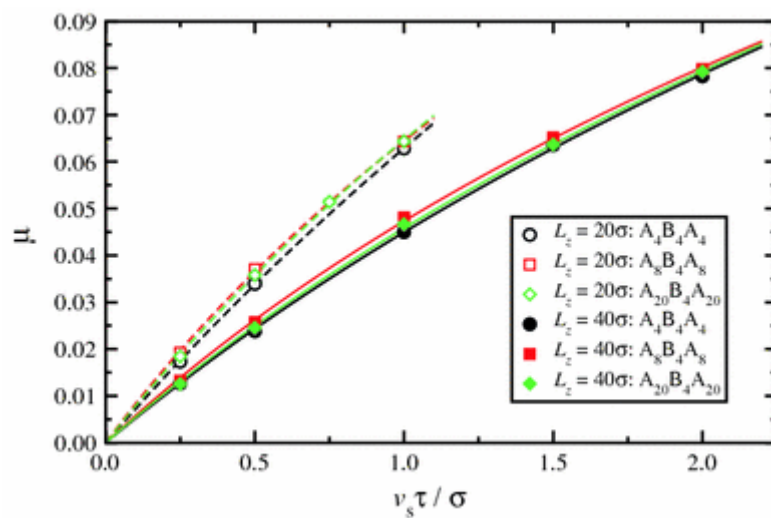
Figure 10. Kinetic friction coefficient μ against sliding velocity v_s for systems with $L_z = 20\,\sigma$ (*open symbols and dashed lines*) and $L_z = 40\,\sigma$ (*filled symbols and solid lines*) and with equal

concentrations of molecular B_4 units: $6\%A_4B_4A_4$ in oil (*black circles*); $10\%A_8B_4A_8$ in oil (*red squares*); $22\%A_{20}B_4A_{20}$ in oil (*green diamonds*)

4. Summary

Molecular simulations have been used to study the influence of additive molecules on the kinetic friction in thin layers of oil confined between parallel walls. The key features of some current additive molecules are the presence of solvophilic chains (aliphatic chains) and solvophobic sections (polar groups). In this work, the molecules were represented using coarse-grained, bead-spring models that reflect the solvophobic and solvophilic characteristics of different parts of the molecules. In particular, the solvophobic sections experience effective attractions with each other (analogous to the hydrophobic attraction between non-polar media in water) and attractions with the surfaces. The kinetic friction coefficient was measured as a function of wall separation, sliding velocity, molecular weight and architecture, and oil–additive composition.

For all of the systems simulated, the results suggest that the kinetic friction coefficient increases first linearly and then logarithmically with increasing sliding velocity. This is in line with earlier work at high sliding velocities [6, 17, 18, 19, 20]; in the current case, though, an empirical equation interpolating between the linear and logarithmic regimes was found to give excellent fits.

A comparison of results for additive molecules with $A_nB_4A_n$ architecture (with A and B representing solvophilic and solvophobic groups, respectively) and equal volume fraction shows that there is an optimum molecular weight for increasing friction. Medium-weight molecules (roughly corresponding to aliphatic chains of 20 methylene units) outperform light-weight (10 methylene) and heavy-weight (50 methylene) analogues. From plots of the distribution of additive across the fluid layer, it was shown that a stratified spanning structure correlates with an increase in friction. The medium-weight additive molecules possess the right degree of solvation in the oil and association between the polar groups to span the fluid layer. Heavy-weight molecules appear to be distributed primarily near the walls, leading to a lubricating layer which does not increase friction.

The effects of molecular architecture were also shown to be important. For the medium-weight molecules, the connectivity of the solvophilic and solvophobic groups was seen to be a key factor. The $A_8B_4A_8$ additive molecules were elongated and adopted the important spanning structure, giving rise to higher friction than the $A_{16}B_4$ variant which was not as elongated and was distributed almost uniformly across the layer. The elongation of the solvophilic chains and the reduction in crowding of the solvophobic groups is possibly a prerequisite for effective additive association. On entropic

grounds, a greater force is required to elongate longer chains, so this might be the reason why it is better to have two shorter solvophilic chains (for solvation and ease of elongation).

Given the importance of additive association, it might have been the case that the concentration of solvophobic groups dictates the increase in friction. In fact, for AnB$_4$An molecules this was shown to not be true. For a given concentration of solvophobic groups, the medium-weight molecule was still superior to the light-weight and heavy-weight analogues, showing that the crucial factor is getting the right balance between oil–additive solvation and additive–additive attractions.

This section concludes with a comment on future work. An important modification of the simulation models used here could be a more faithful representation of the surface and in particular its roughness. The level surfaces used here lead to rather low values of the kinetic friction, although at the highest sliding velocities, they are certainly of the right order of magnitude ($\sim$0.1). The sliding velocities explored in this study, although being in line with those applied in earlier work on nanoscale fluid layers [4, 6, 9], are rather high. This does not appear to have been a problem for this study, which has focused on comparing the effects of different additive molecules. The forces in the direction of shear can easily be increased by making the surfaces rough. This can be done in a variety of ways, but for a given application the surface topology and degree of roughness should be explored experimentally and then an appropriate simulation model can be constructed.

References

[1] Tarasov, S., Kolubaev, A., Belyaev, S., Lerner, M., Tepper, F.: Study of friction reduction by nanocopper additives to motor oil. *Wear* **252**, 63–69 (2002).

[2] Wu, Y.Y., Tsui, W.C., Liu, T.C.: Experimental analysis of tribological properties of lubricating oils with nanoparticle additives. *Wear* **262**, 819–825 (2007).

[3] Scott, W., Suntiwattana, P.: Effect of oil additives on the performance of a wet friction clutch material. *Wear* **181**(183), 850–855 (1995).

[4] Thompson, P.A., Robbins, M.O.: Shear-flow near solids - epitaxial order and flow boundary-conditions. *Phys. Rev. A* **41**, 6830–6837 (1990).

[5] He, G., Müser, M.H., Robbins, M.O.: Adsorbed layers and the origin of static friction. *Science* **284**, 1650–1652 (1999).

[6] He, G., Robbins, M.O.: Simulations of the kinetic friction due to adsorbed surface layers. *Tribol Lett* **10**, 7–14 (2001).

[7] He, G., Robbins, M.O.: Simulations of the static friction due to adsorbed molecules. *Phys. Rev. B* **64**, 035413 (2001).

[8] Müser, M.H., Wenning, L., Robbins, M.O.: Simple microscopic theory of Amontons' laws for static friction. *Phys. Rev. Lett.* **86**, 1295–1298 (2001).

[9] Barsky, S., Robbins, M.O.: Bulk and interfacial shear thinning of immiscible polymers. *Phys. Rev. E* **65**, 021808 (2002).

[10] Müser, M.H., Urbakh, M., Robbins, M.O.: Statistical mechanics of static and low-velocity kinetic friction. *Adv. Chem. Phys.* **126**, 187–272 (2003).

[11] Gao, J., Luedtke, W.D., Gourdon, D., Ruths, M., Israelachvili, J.N., Landman, U.: Frictional forces and Amontons' law: From the molecular to the macroscopic scale. *J. Phys. Chem. B* **108**, 3410–3425 (2004).

[12] Gao, J., Luedtke, W.D., Landman, U.: Friction control in thin-film lubrication. *J. Phys. Chem.* B **102**, 5033–5037 (1998).

[13] Sivebaek, I.M., Samoilov, V.N., Persson, B.N.J.: Frictional properties of confined polymers. Euro. *Phys. J. E* **27**, 37–46 (2008).

[14] Bitsanis, I.A., Pan, C.: The origin of "glassy" dynamics at solid-oligomer interfaces. *J. Chem. Phys.* **99**, 5520–5527 (1993).

[15] Manias, E., Hadziioannou, G., Tenbrinke, G.: Effect of shear on the desorption of oligomers in nanoscopically confined fluids. *J. Chem. Phys.* **101**, 1721–1724 (1994).

[16] Hirz, S., Subbotin, A., Frank, C., Hadziioannou, G.: Static and kinetic friction of strongly confined polymer films under shear. *Macromolecules* **29**, 3970–3974 (1996).

[17] Dieterich, J.H.: Modeling of rock friction. 1. Experimental results and constitutive equations. *J. Geophys. Res.* **84**, 2161–2168 (1979).

[18] Dieterich, J.H.: Modeling of rock friction. 2. Simulation of pre-seismic slip. *J. Geophys. Res.* **84**, 2169–2175 (1979).

[19] Ruina, A.: Slip instability and state variable friction laws. *J. Geophys. Res.* **88**, 359–370 (1983).

[20] Gu, J.C., Rice, J.R., Ruina, A.L., Tse, S.T.: Slip motion and stability of a single degree of freedom elastic system with rate and state dependent friction. *J. Mech. Phys. Sol.* **32**, 167–196 (1984).

[21] Perez, D., Dong, Y., Martini, A., Voter, A.F.: Rate theory description of atomic stick-slip friction. *Phys. Rev. B* **81**, 24515 (2010).

[22] Greenfield, M.L., Ohtani, H.: Molecular dynamics simulation study of model friction modifier additives confined between two surfaces. *Tribol. Lett.* **7**, 137–145 (1999).

[23] Onodera, T., Morita, Y., Suzuki, A., Koyama, M., Tsuboi, H., Hatakeyama, N., Endou, A., Takaba, H., Kubo, M., Dassenoy, F., Minfray, C., Joly-Pottuz, L., Martin, J.M., Miyamoto, A.: A computational chemistry study on friction of h-MoS_2. Part I. Mechanism of single sheet lubrication. *J. Phys. Chem. B* **113**, 16526–16536 (2009).

[24] Onodera, T., Morita, Y., Nagumo, R., Miura, R., Suzuki, A., Tsuboi, H., Hatakeyama, N., Endou, A., Takaba, H., Dassenoy, F., Minfray, C., Joly-Pottuz, L., Kubo, M., Martin, J.M., Miyamoto, A.: A computational chemistry study on friction of h-MoS_2. Part II. Friction anisotropy. *J. Phys. Chem. B* **114**, 15832–15838 (2010).

[25] Berro, H., Fillot, N., Vergne, P.: Molecular dynamics simulation of surface energy and ZDDP effects on friction in nano-scale lubricated contacts. *Tribology International* **43**, 1811–1822 (2010).

[26] Confidential experimental information from Infineum UK Ltd.

[27] Chandler, D.: Interfaces and the driving force of hydrophobic assembly. *Nature* **437**, 640–647 (2005).

[28] Grest, G.S., Kremer, K.: Molecular dynamics simulation for polymers in the presence of a heat bath. *Phys. Rev. A* **33**, 3628–3631 (1986).

[29] Grest, G.S., Kremer, K., Witten, T.A.: Structure of many-arm star polymers: a molecular dynamics simulation. *Macromolecules* **20**, 1376–1383 (1987).

[30] Grest, G.S., Lacasse, M.D., Kremer, K., Gupta, A.M.: Efficient continuum model for simulating polymer blends and copolymers. *J. Chem. Phys.* **105**, 10583–10594 (1996).

[31] Nielsen, S.O., Lopez, C.F., Srinivas, G., Klein, M.L.: Coarse grain models and the computer simulation of soft materials. *J. Phys.* **16**, R481–R512 (2004).

[32] Peter, C., Kremer, K.: Multiscale simulation of soft matter systems. *Faraday Discuss.* **144**, 9–24 (2010).

[33] Materials Studio 4.2, Accelrys Inc., San Diego, CA 92121.

[34] Hansen, J.P., McDonald, I.R.: *Theory of Simple Liquids.* Academic Press, London (1986).

[35] Weeks, J.D., Chandler, D., Andersen, H.C.: Role of repulsive forces in determining the equilibrium structure fo simple liquids. J. Chem. Phys. **54**, 5237–5247 (1971).

[36] Priezjev, N.V.: Relationship between induced fluid structure and boundary slip in nanoscale polymer films. *Phys. Rev. E* **82**, 051603 (2010).

[37] Allen, M.P., Tildesley, D.J.: *Computer Simulation of Liquids.* Clarendon Press, Oxford (1987).

[38] Martini, A., Dong, Y., Perez, D., Voter, A.F.: Low-speed atomistic simulation of stick-slip friction using parallel replica dynamics. *Tribol. Lett.* **36**, 63–68 (2009).

[39] Eyring, H.: Viscosity, plasticity, and diffusion as examples of absolute reaction rates. *J. Chem. Phys.* **4**, 283–291 (1936).

[40] Martini, A., Hsu, H.Y., Patankar, N.A., Lichter, S.: Slip at high shear rates. *Phys. Rev. Lett.* **100**, 206001 (2008).

[41] Rubinstein, M., Colby, R.H.: *Polymer Physics.* Oxford University Press, Oxford (2003).